Adv. Polar Upper Atmos. Res., **20**, 000-000, 2006

Neutral atom emission coming from the direction of the high-latitude magnetopause under northward IMF

Satoshi Taguchi[1], Keisuke Hosokawa[1], Yozo Murata[2], Akira Nakao[1],

Michael R. Collier[3], Thomas E. Moore[3],

Natsuo Sato[4], and A. Sessai Yukimatu[4]

[1]*Department of Information and Communication Engineering, University of Electro-Communications, Chofu-shi, Tokyo, 182-8585*

[2] *Sugadaira Space Radio Observatory, University of Electro-Communications, Chofu-shi, Tokyo, 182-8585*

[3] *NASA Goddard Space Flight Center, Greenbelt, MD 20771, U.S.A.*

[4] *National Institute of Polar Research, Itabashi-ku, Tokyo, 173-8515*

Abstract: The Low Energy Neutral Atom (LENA) imager on the Imager for Magnetopause-to-Aurora Global Exploration (IMAGE) spacecraft in the magnetosphere can detect neutral particles coming from the direction of the magnetopause. During a period of dynamic pressure of ~6 nPa and IMF B_Z of ~15 nT on March 27, 2001, significant neutral atom emissions occurred in the direction of the very high-latitude magnetopause. Simultaneous observations from IMAGE/LENA and SuperDARN radar show that the LENA emission appears concurrently with the enhancement of the sunward flow of the reverse convection in the ionosphere. In a recent paper (Taguchi *et al*., Geophysical Research Letters, 2006) this type of emission has been interpreted as being produced by the fast ion flow caused by cusp reconnection through charge exchange with the Earth's hydrogen exosphere. In other words, remote sensing using LENA imager can be applied in order to determine the stability of the reconnection site. From results of analyses of LENA emission data we show that the reconnection "spot" mapped on a sphere having a radius of 8 R_E shifts tailward by approximately 1 R_E over 10 minutes while fluctuating.

Key words: Cusp, neutral atoms, reconnection, and IMF

1. Introduction

In situ spacecraft observations have established the presence of reconnection that is operative poleward of the cusp for northward interplanetary magnetic field (IMF) (*e.g.* Gosling *et al*., 1991). This cusp reconnection drives reverse convection, which consists of sunward flow in the dayside polar cap and return flow at lower latitudes. The reconnection also causes magnetosheath ions to enter such a sunward convection region. In this region, ions with higher energies appear at high latitudes, and lower energy ions arrive at somewhat lower latitudes, demonstrating reversed ion dispersion. The speed of the fast ion flow at the high-latitude edge has been observed to be 200-400 km s^{-1} by the Polar (*e.g.* Fuselier *et al*., 2000) and the Cluster spacecraft (*e.g.* Phan *et al*., 2003).

One of the important issues about this fast flow is to understand the degree to which this flow layer exists stably during northward IMF. However, it is difficult to examine the stability of this phenomenon by in situ spacecraft observations because spacecraft usually reside in that layer for only a few minutes. Fuselier *et al*. (2000) proposed an interesting approach, in which the distance to the reconnection site from the location of the in situ Polar observation is estimated by proton distributions having characteristic low-energy cutoffs. In addition, the stability of the reconnection site for a few tens of minutes has been discussed. However, in order to further our understanding, considering the fact that there are large uncertainties in the method based on the proton distributions from the in situ observation, a remote-sensing approach is required.

Remote sensing using the Low Energy Neutral Atom (LENA) imager (Moore *et al*., 2000) on the IMAGE spacecraft can be used to understand the distribution of the ion flow in the region where significant source ions, which can produce neutral atom emissions through charge exchange with the Earth's hydrogen exosphere, are present.

Several studies using LENA have shown that significant source ions are present in either the post-shocked flow of the solar wind (Collier *et al*., 2001a, 2001b), in the magnetosheath flow near the subsolar magnetopause (Collier *et al*., 2001a; Moore *et al*., 2003; Fok *et al*., 2003; Taguchi *et al*., 2004a; Collier *et al*., 2005) or the flow in the cusp indentation (Taguchi *et al*., 2004a, 2004b), as well as in the outflow from the ionosphere (*e.g.* Moore *et al*., 2001; Fuselier *et al*., 2002; Khan *et al*., 2003; Wilson *et al*., 2003, 2005; Nosé *et al*., 2005).

In addition, recent two studies with the LENA imager have shown that LENA can be also applied to understand the dynamics of the ion entry equatorward or poleward edge of the cusp (Taguchi *et al*., 2005, 2006). Using simultaneous observations from IMAGE and Polar, Taguchi *et al*. (2005) have shown that the LENA fluxes in the direction of the cusp are composed of relatively stable high latitude and flickering low latitude emissions, and that the low latitude emissions are associated with the ion entry on the equatorward edge of the cusp for southward IMF. Analyzing a significant LENA emission event during strongly northward IMF, Taguchi *et al*. (2006) has interpreted the LENA emission in the direction of the very high-latitude magnetopause as being due to the cusp reconnection that is operative for northward IMF.

The cusp reconnection causes magnetosheath ions to enter the magnetosphere. The fast ion flow from the reconnection site produces the neutral atom through charge exchange with the Earth's hydrogen exosphere if it enters a region of adequate hydrogen density. The neutral atom emission is detected by the LENA imager when IMAGE is located downstream of the ion entry (Figure 4 in Taguchi *et al*., 2006). Hence, enhanced neutral atom emission is observed coming from the direction of the very high-latitude magnetopause when IMF is northward.

In the present study, we extend the above study (Taguchi *et al*., 2006) by analyzing LENA data in detail focusing on the initial 24 min interval out of a significant LENA

emission event on 27 March 2001. We show that the LENA reconnection "spot" mapped onto a sphere with a radius of 8 R_E shifts tailward by about 1 R_E over ~10 minutes while fluctuating.

2. Overview of Observations on 27 March 2001

Figures 1a and 1b show the IMAGE orbit in the X_{GSM}-Z_{GSM} and X_{GSM}-Y_{GSM} planes for 1730 - 1940 UT. At 1730 UT, IMAGE was located near (X_{GSM}, Z_{GSM}) ~ (2.7 R_E, 7.4 R_E) in the mid-noon sector (Y_{GSM} ~ 0 R_E). In Figure 1a the outermost solid curve represents the magnetopause predicted by Shue *et al.* (1998) with the IMF B_Z of 15 nT and a dynamic pressure of 6 nPa, which are representative ACE solar wind conditions for this event. It appears that IMAGE is well inside the magnetopause.

Figure 1a also shows the radial distance of 8 R_E (dotted curve). Inside this radial distance, approximately, the exospheric neutral hydrogen densities increase sharply with the decrease in the geocentric distance, as compared to the density profiles outside this distance (Østgaard *et al.*, 2003). Since IMAGE is inside this distance, it is expected that the neutral atom emission due to charge-exchange of ions with the Earth hydrogen exosphere can be detected from altitudes above and below the spacecraft.

During the interval of interest, the SuperDARN radar (Greenwald *et al.*, 1995) at Saskatoon, Canada (52.16°N, 106.53°W) monitored plasma convection near the cusp in the ionosphere. Figure 2 shows several examples of the line-of-sight (LOS) velocity maps from Saskatoon radar scans for 40 minutes out of the above period. The field of view covers the daytime sector from ~09 MLT to ~15 MLT, and significant backscatter signals were obtained from the ionosphere between ~09 MLT and ~13 MLT.

The green/blue color in each plot represents the existence of the sunward flow. Throughout the interval the flow is sunward near the local noon and is anti-sunward on the prenoon side, i.e., showing a reverse convection pattern, although the velocities

become somewhat weak at 1848 UT (Figure 2e). We analyzed LENA data for 1820 – 1844 UT during which the emission occurs continuously (shown later). This interval is before the time for Figure 2e and immediately after the time for Figure 2b.

Figure 3 shows variations of ACE solar wind, IMAGE/LENA hydrogen count rate, and LOS velocity obtained using the SuperDARN radar. Panels a-d display the solar wind parameters, which are shifted by 32 min, by relating the ACE detection of an interplanetary shock at 1715 UT with a sudden commencement observed at 1747 UT in the H-component of the SYM index (SYM-H) (Iyemori and Rao, 1996) (Panel e). IMF B_Z (in GSM coordinates) is northward during the most of the plotted interval. Note that the solar wind convection time ~32 min is not constant. The convection time gets several minutes longer at the end of the interval, as is estimated from the comparison between the southward turning of IMF (Panel c) and the change of the ionospheric convection, which is shown later.

Panel f of Figure 3 shows the LENA background-corrected hydrogen data in spectrogram format. The zero degree position in the *Y*-axis represents the direction of the center of the LENA spin angle sector that is the closest to the solar direction for this interval. We refer to the angle on the *Y*-axis as solar spin phase (SSP). The Sun signal (*e.g.* Moore *et al*., 2001; Collier *et al*., 2001a; Collier *et al*., 2003) representing neutral solar wind is clearly identified as a narrow green line near the zero SSP. In this study, we consider LENA emissions at angles much greater than the Sun signal, and relate the emissions to the plasma flow from the SuperDARN. Panel g shows the LOS (poleward) velocity for beam 5 of the SuperDARN Saskatoon radar in the format in which the range gate of the beam is on the *Y*-axis.

The LENA emission for SSP~90°, which comes primarily from the direction of the very high-latitude magnetopause, is enhanced at 1820 UT. The sunward flow (green/blue color in Panel g) in the ionosphere, which is typical of northward IMF, is

enhanced upon the appearance of the LENA emission at 1820 UT. The LOS velocity enhancement at this time is roughly 400 ms^{-1} (Taguchi *et al*., 2006).

At 1926 UT, the emission distribution drastically changes to cover a much wider angle range than the distribution during 1820-1926 UT. Immediately thereafter, anti-sunward flow appears in the ionosphere (Panel g), indicating that the LENA emission no longer exhibits the conditions for northward IMF (Panel c) after this time. This suggests that the northward IMF is associated with the emission for 1820-1926 UT.

From 1820 to 1926 UT, the LENA emission comes primarily from SSP of 90°-150°. Although the direction of the emission is relatively stable, its direction changes slightly so that the emission may shift to higher or lower SSP. Shortly after the emission begins, it spreads over a wider SSP range (from 60° to 200°) around 1830 UT. The SSP then increases during the period from ~1830 to ~1845 UT. There is no clear variation in SSP for ~1848 to ~1910 UT. During the period from 1918 to 1926 UT the emission moves to lower angles.

3. Temporal Variations of LENA Snapshots

Taguchi *et al*. (2005, 2006) have presented LENA snapshots in a format in which the hydrogen count rate for each line of sight is plotted on a sphere having a radius of 8 R_E. Since inside this radial distance, approximately, the exospheric neutral hydrogen densities increase sharply with the decrease in the geocentric distance, as compared to the density profiles outside this distance (Østgaard *et al*., 2003), the choice of this sphere as a mapping surface for the emission coming from altitudes above the spacecraft (at $R \sim 7R_E$) appears to be reasonable.

Using the Tsyganenko 96 model, Taguchi *et al*. (2006) have also shown that the peak of the LENA emission on this sphere is mapped down to the sunward flow region of the reverse convection in the dayside ionosphere. This suggests that the source ions

for the LENA emission are in the magnetospheric counterpart of the sunward flow of the reverse convection. This type of LENA emission has been interpreted as being due to the fast ion flow caused by cusp reconnection (Taguchi *et al*., 2006).

The fast ion flow from the cusp reconnection produces the neutral atom through charge exchange with the Earth's hydrogen exosphere if it enters a region of adequate hydrogen density. The neutral atom emission is detected by the LENA imager when spacecraft is located downstream of the ion entry (Figure 4 in Taguchi *et al*., 2006). In other words, LENA can monitor the ion entry caused by cusp reconnection. Note that the present analysis does not show any information on the distance between the cusp reconnection site on the magnetopause and the 8 R_E sphere.

Two examples of LENA snapshots (at 1828 UT and at 1838 UT) are shown in Figures 4a and 4b, respectively. In Figure 4a, the peak of the emission can be seen at (X,Y,Z) = (3.1, –0.1, 7.4) R_E on the sphere having a radius of 8 R_E. Ten minutes later, in Figure 4b, the peak of the emission can be identified at (X,Y,Z) = (2.5, –0.3, 7.6) R_E. The emission appears to have shifted tailward. In these figures the width of the mapping surface is narrow around X_{GSM}~4 R_E when compared with that for X_{GSM}~0. This simply reflects that the mapping surface for the LENA field of view looking into X_{GSM}~4 R_E is relatively close to the location of the spacecraft.

Figure 5 shows the temporal variations of the X_{GSM} position of the LENA peak emission on the 8 R_E sphere from 1820 UT to 1844 UT. This period corresponds to the first interval of continuous significant LENA emissions during the present event (see Figure 3f). To identify the peak emission, we first found an SSP sector (with an 8° spin angle) showing a maximum count peak in the range of 56° – 154°, and then determined the maximum count bin among 12 polar angle bins constituting this SSP sector. The location of the peak emission appears to be stable during the former half of the interval. However, in the latter half, the location moves toward a smaller X_{GSM} while fluctuating.

The emission shifts tailward by approximately 1 R_E over 10 minutes. Note that the signal at the sudden change in X_{GSM} (1842 UT) still has significant brightness (Panel f of Figure 3).

4. Concluding Remarks

Gosling *et al.* (1991) have pointed out that if reconnection is initiated at high-latitudes tailward of the site at which the magnetosheath flow becomes super-Alfvénic, the reconnection site moves tailward so that the magnetosheath flow is Alfvénic in the deHoffman-Teller frame. Even if such tailward motion occurs, the injected ions remain along similar magnetic field lines on the high-latitude magnetopause, and no significant change in the reconnection spot on the 8 R_E sphere would occur.

Another possible cause of the tailward shift is the compression of the high-latitude magnetopause. When the high-latitude magnetopause is pushed inward, the reconnection site can also be moved inward (i.e., in the tailward direction). The injected ions can then be observed in a somewhat tailward position on the 8 R_E sphere. In this case, the solar wind dynamic pressure would be expected to increase with the tailward motion of the reconnection spot. However, the temporal variation of the location of the reconnection spot is not similar to that of the ACE dynamic pressure (in Panel d of Figure 3).

Taguchi *et al*. (2006) have suggested that, in addition to a strong northward IMF, an IMAGE location having a large Z and a relatively large solar wind density are necessary to monitor the cusp reconnection. From the noon-midnight passes for the period from March to April 2001, Taguchi *et al*. (2006) have found two events in addition to the present event by searching for intervals having an ACE solar wind density greater than 15 cm^{-3}, an ACE IMF B_Z greater than 15 nT, and an IMAGE Z_{GSM}

greater than 5 R_E. Detailed examination of these two additional events will be performed in the next step. Combined analyses of these three events would help to clarify the reason for the tailward motion of the reconnection site.

Acknowledgements

This research was supported by grant-in-aid 15540427 and 18540443 in Category C under Japan Society for the Promotion of Science, and by the IMAGE Project under UPN 370-28-20 at Goddard Space Flight Center. Operation of the Saskatoon radar is supported by an NSERC Major Facilities Access Grant and a Canadian Space Agency contract. ACE solar wind data are provided by NASA/NSSDC. The authors thank D. McComas (PI of ACE plasma data), and N. Ness (PI of ACE magnetic field data). We also thank WDC for Geomagnetism, Kyoto, Japan for providing the midlatitude SYM-H index.

References

Collier, M.R., Moore, T.E., Fok, M.-C., Pilkerton, B., Boardsen, S. and Khan, H. (2005): Low-energy neutral atom signatures of magnetopause motion in response to southward B_z. J. Geophys. Res., **110**, A02102, doi:10.1029/2004JA010626.

Collier, M.R., Moore, T.E., Ogilvie, K., Chornay, D.J., Keller, J., Fuselier, S., Quinn, J., Wurz, P., Wuest, M. and Hsieh, K.C. (2003): Dust in the wind: The dust geometric cross section at 1 AU based on neutral solar wind observations. Solar wind ten, Proc. of the tenth Int. Solar Wind Conf., Velli, M., Bruno, R. and Malara, F. (eds.), AIP Conf., **679**, 790–793.

Collier, M.R., Moore, T.E., Fok, M.-C., Chornay, D., Rastaetter, L., Kuznetsova, M., Falasca, A., Green, J., Boardsen, S., Fuselier, S., Petrinec, S., Thomsen, M., McComas, D. and Gombosi, T.I. (2001a): LENA observations on March 31, 2001: Magnetosheath remote sensing. Eos. Trans. AGU, **82**(47), Fall Meeting Suppl., Abstract SM41C-05, F1071-F1072.

Collier, M.R., Moore, T.E., Ogilvie, K.W., Chornay, D., Keller, J.W., Boardsen, S., Burch, J., Marji, B.E., Fok, M.-C., Fuselier, S.A., Ghielmetti, A.G., Giles, B.L., Hamilton, D.C., Peko, B.L., Quinn, J.M., Roelof, E.C., Stephen, T.M., Wilson, G.R. and Wurz, P. (2001b): Observations of neutral atoms from the solar wind. J. Geophys. Res., **106**, 24893-24906.

Fok, M.-C., Moore, T.E., Wilson, G.R., Perez, J.D., Zhang, X.X., Brandt, P.C:son, Mitchell, D.G., Roelof, E.C., Jahn, J.-M., Pollock, C.J. and Wolf, R.A. (2003): Global ENA IMAGE simulations. Space Sci. Rev., **109**, 77-103.

Fuselier, S.A., Petrinec, S.M. and Trattner, K.J. (2000): Stability of the high-latitude reconnection site for steady northward IMF. Geophys. Res. Lett., **27**, 473-476.

Fuselier, S.A., Collin, H.L., Ghielmetti, A.G., Claflin, E.S., Moore, T.E., Collier, M.R., Frey, H. and Mende, S.B. (2002): Localized ion outflow in response to a solar wind pressure pulse. J. Geophys. Res., **107**, No. A8, 10.1029/2001JA000297.

Gosling, J.T., Thomsen, M.F., Bame, S.J., Elphic, R.C. and Russell, C.T. (1991): Observations of reconnection of interplanetary and lobe magnetic field lines at the high-latitude magnetopause. J. Geophys. Res., **96**, 14097-14106.

Greenwald, R.A., Baker, K.B., Dudeney, J.R., Pinnock, M., Jones, T.B., Thomas, E.C., Villain, J.-P., Cerisier, J.-C., Senior, C., Hanuise, C., Hunsucker, R.D., Sofko, G., Koehler, J., Nielsen, E., Pellinen, R., Walker, A.D.M., Sato, N. and Yamagishi, H. (1995): DARN/SuperDARN: A global view of the dynamics of high-latitude convection. Space Sci. Rev., **71**, 761-796.

Iyemori, T. and Rao, D.R.K. (1996): Decay of the *Dst* component of geomagnetic disturbance after substorm onset and its implication to storm substorm relation. Ann. Geophys., **14**, 608-618.

Khan, H., Collier, M.R. and Moore, T.E. (2003): Case study of solar wind pressure variations and neutral atom emissions observed by IMAGE/LENA. J. Geophys. Res., **108**(A12), 1422, doi:10.1029/2003JA009977.

Moore, T.E., Collier, M.R., Fok, M.-C., Fuselier, S.A., Khan, H., Lennartsson, W., Simpson, D.G., Wilson, G.R. and Chandler, M.O. (2003): Heliosphere-Geosphere interactions using Low Energy Neutral Atom imaging, Space Sci. Rev., **109**, 351-371.

Moore, T.E., Collier, M.R., Burch, J.L., Chornay, D.J., Fuselier, S.A., Ghielmetti, A.G., Giles, B.L., Hamilton, D.C., Herrero, F.A., Keller, J.W., Ogilvie, K.W., Peko, B.L., Quinn, J.M., Stephen, T.M., Wilson, G.R. and Wurz, P. (2001): Low energy neutral atoms in the magnetosphere. Geophys. Res. Lett., **28**, 1143-1146.

Moore, T.E., Chornay, D.J., Collier, M.R., Herrero, F.A., Johnson, J., Johnson, M.A., Keller, J.W., Laudadio, J.F., Lobell, J.F., Ogilvie, K.W., Rozmarynowski, P., Fuselier,

S.A., Ghielmetti, A.G., Herzberg, E., Hamilton, D.C., Lundgren, R., Wilson, P., Walpole, P., Stephen, T.M., Peko, B.L., Zyl, B.Van, Wurz, P., Quinn, J.M. and Wilson, G.R. (2000): The low-energy neutral atom imager for IMAGE. Space Sci. Rev., **91**, 155-195.

Nosé, M., Taguchi, S., Hosokawa, K., Christon, S.P., McEntire, R.W., Moore, T.E. and Collier, M.R. (2005): Overwhelming O^+ contribution to the plasma sheet energy density during the October 2003 superstorm: Geotail/EPIC and IMAGE/LENA observations. J. Geophys. Res., **110**, A09S24, doi:10.1029/2004JA010930.

Østagaard, N., Mende, S.B., Frey, H.U., Gladstone, G.R. and Lauche, H. (2003): Neutral hydrogen density profiles derived from geocoronal imaging. J. Geophys. Res., **108**, doi:10.1029/2002JA009749.

Phan, T. *et al*., (2003): Simultaneous Cluster and IMAGE observations of cusp reconnection and auroral proton spot for northward IMF. Geophys. Res. Lett., **30**(10), 1509, doi:10.1029/2003GL016855.

Shue, J.-H., Song, P., Russell, C.T., Steinberg, J.T., Chao, J.K., Zastenker, G., Vaisberg, O.L., Kokubun, S., Singer, H.J., Detman, T.R. and Kawano, H. (1998): Magnetopause location under extreme solar wind conditions. J. Geophys. Res., **103**, 17691-17700.

Taguchi, S., Collier, M.R., Moore, T.E., Fok, M.-C. and Singer, H.J. (2004a): Response of neutral atom emissions in the low- and high-latitude magnetosheath direction to the magnetopause motion under extreme solar wind conditions. J. Geophys. Res., **109**, A04208, doi:10.1029/2003JA010147.

Taguchi, S., Chen, S.-H., Collier, M.R., Moore, T.E., Fok, M.-C., Hosokawa, K. and Nakao, A. (2005): Monitoring the high-altitude cusp with the Low Energy Neutral Atom imager: Simultaneous observations from IMAGE and Polar. J. Geophys. Res., **110**, A12204, doi:10.1029/2005JA011075.

Taguchi, S., Hosokawa, K., Collier, M.R., Moore, T.E., Fok, M.-C., Yukimatu, A.S., Sato, N. and Greenwald, R.A. (2004b): Simultaneous observations of the cusp with IMAGE Low Energy Neutral Atom imager and SuperDARN radar. Adv. Polar Upper Atmos. Res., **18**, 53-64.

Taguchi, S., Hosokawa, K., Nakao, A., Collier, M.R., Moore, T.E., Yamazaki, A., Sato, N. and Yukimatu, A.S. (2006): Neutral atom emission in the direction of the high-latitude magnetopause for northward IMF: Simultaneous observations from IMAGE spacecraft and SuperDARN radar. Geophys. Res. Lett., **33**, L03101, doi:10.1029/2005GL025020.

Wilson, G. R., and Moore, T. E. (2005): Origins and variation of terrestrial energetic neutral atoms outflow, J. Geophys. Res., **110**, A02207, doi:10.1029/2003JA010356.

Wilson, G. R., Moore, T. E., and Collier, M. (2003): Low-energy neutral atoms observed near the Earth, J. Geophys. Res., **108**(A4), 1142, doi:10.1029/ 2002JA009643.

Figure Captions

Figure 1. IMAGE orbit in the (a) X_{GSM}-Z_{GSM} and (b) X_{GSM}-Y_{GSM} during the interval of 1730-1940 UT, 27 March 2001. The diamond represents the location of IMAGE at 1730 UT. The dotted curve shows the radial distance of 8 R_E, and the outermost solid curve represents the magnetopause predicted by Shue *et al*. (1998).

Figure 2. Line-of-sight velocity maps from Saskatoon Canada radar scans. Blue/green color means the existence of the sunward flow. The sunward flow can be seen near local noon, showing a reverse convection pattern, which is typical of northward IMF.

Figure 3. (a) ACE plasma density, (b) velocity, (c) three components of IMF in GSM, (d) dynamic pressure, (e) SYM-H index, (f) LENA spectrogram, (g) line of sight velocity for beam 5 at the SuperDARN Saskatoon radar. In Panel c 64-s averages of IMF data that were created from original 16-s averages are plotted so as to make comparison between the IMF and plasma data easier. In Panels g gray color simply represents the ground scatter.

Figure 4. Two examples of LENA snapshots observed in the direction of the very high-latitude magnetopause. Background-corrected hydrogen count rates are plotted on the sphere having a radius of 8 R_E. The peak of the emission is indicated with the white cross mark.

Figure 5. Temporal variations of the X_{GSM} position of the LENA peak emission in the direction of the very high-latitude magnetopause. A smaller X_{GSM} means that the emission appears tailward on the sphere having a radius of 8 R_E.

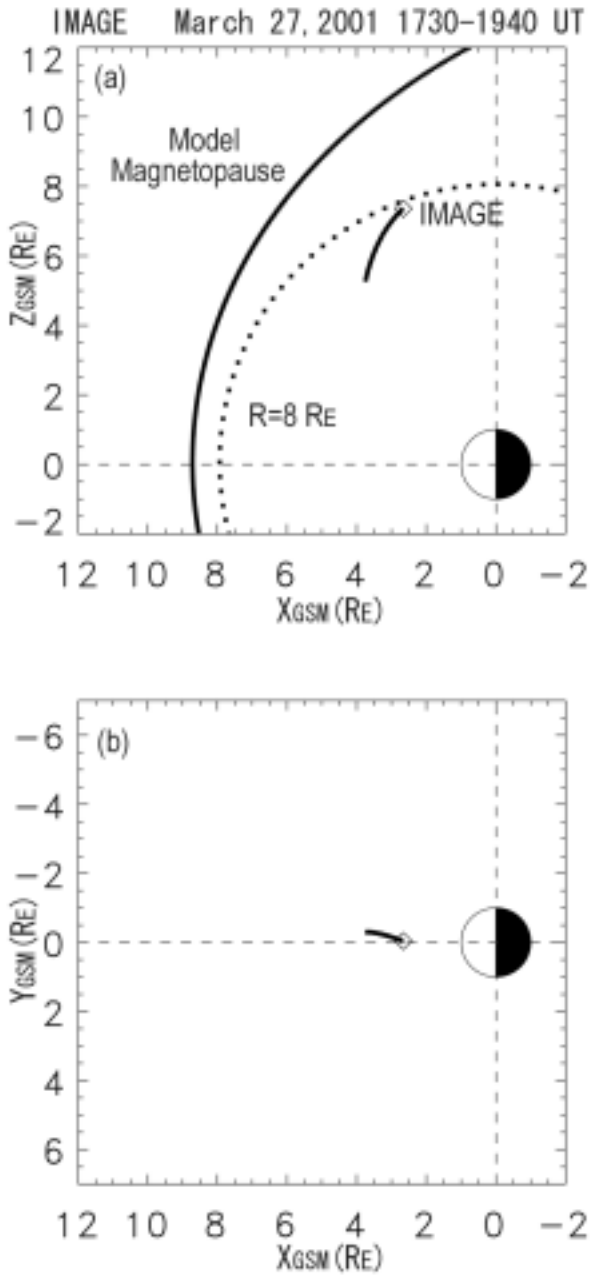
IMAGE March 27, 2001 1730-1940 UT
(a)
Model
Magnetopause
IMAGE
R=8 RE
ZGSM (RE)
XGSM (RE)
(b)
YGSM (RE)
XGSM (RE)

Figure 1.

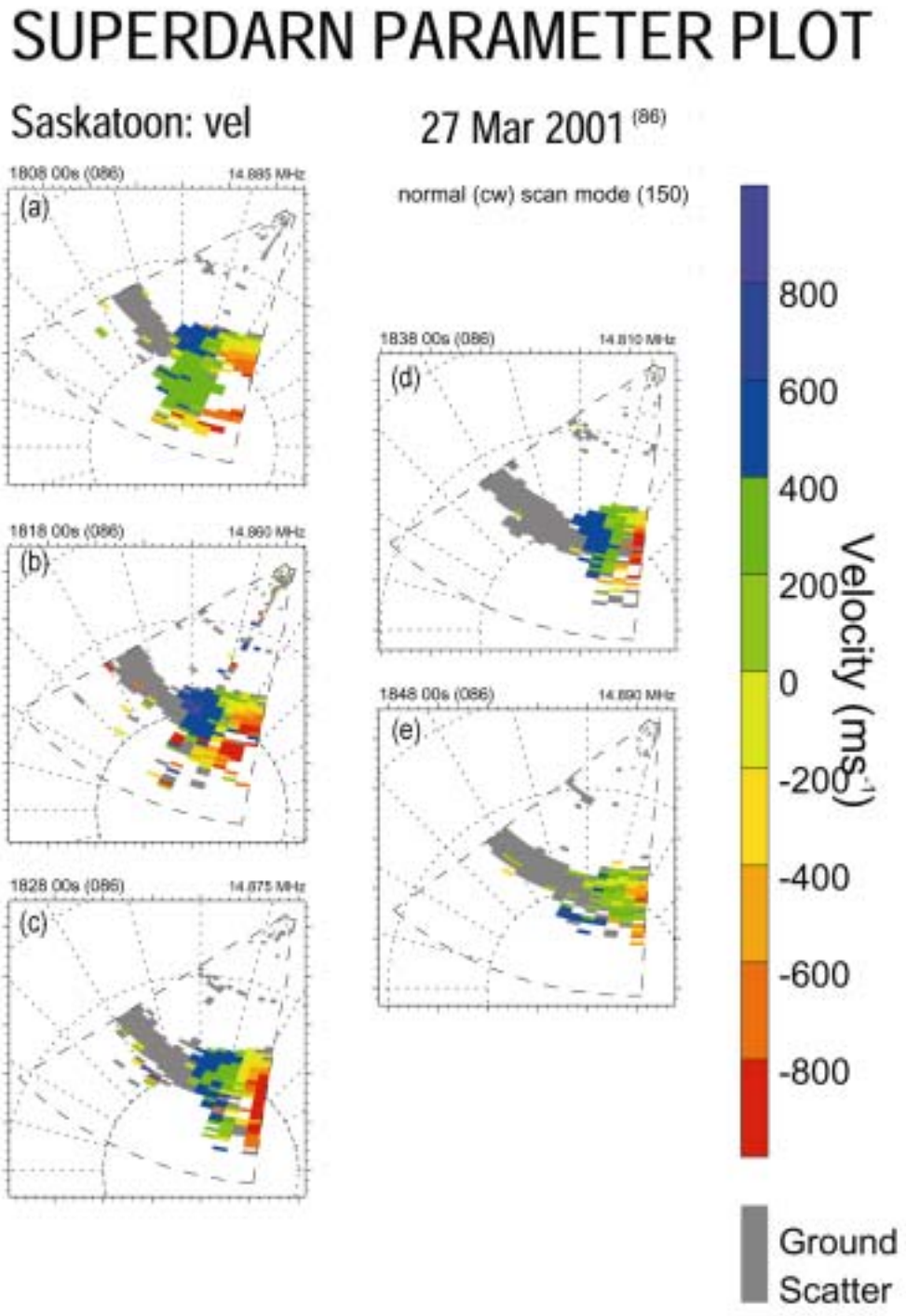
SUPERDARN PARAMETER PLOT
Saskatoon: vel
27 Mar 2001 (86)
normal (cw) scan mode (150)
1808 00s (086)
14.885 MHz
(a)
1818 00s (086)
14.860 MHz
(b)
1828 00s (086)
14.875 MHz
(c)
1838 00s (086)
14.810 MHz
(d)
1848 00s (086)
14.890 MHz
(e)
800
600
400
200
0
-200
-400
-600
-800
Velocity (ms-1)
Ground
Scatter

Figure 2.

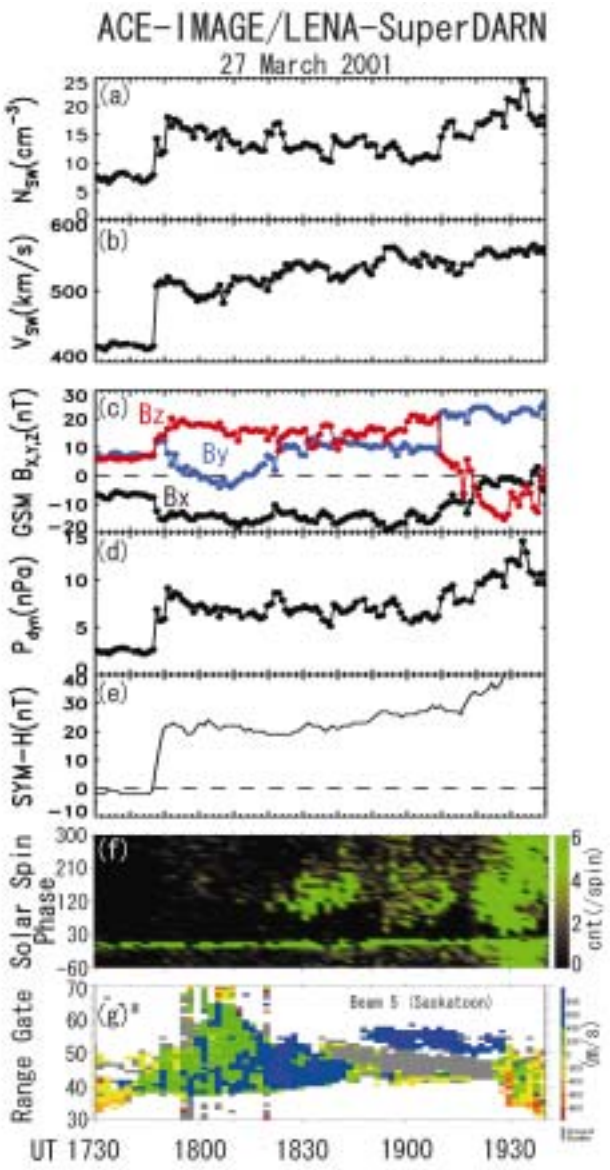
ACE-IMAGE/LENA-SuperDARN
27 March 2001
(a)
(b)
(c)
Bz
By
Bx
(d)
(e)
(f)
(g)
Beam 5 (Saskatoon)
UT 1730
1800
1830
1900
1930

Figure 3.

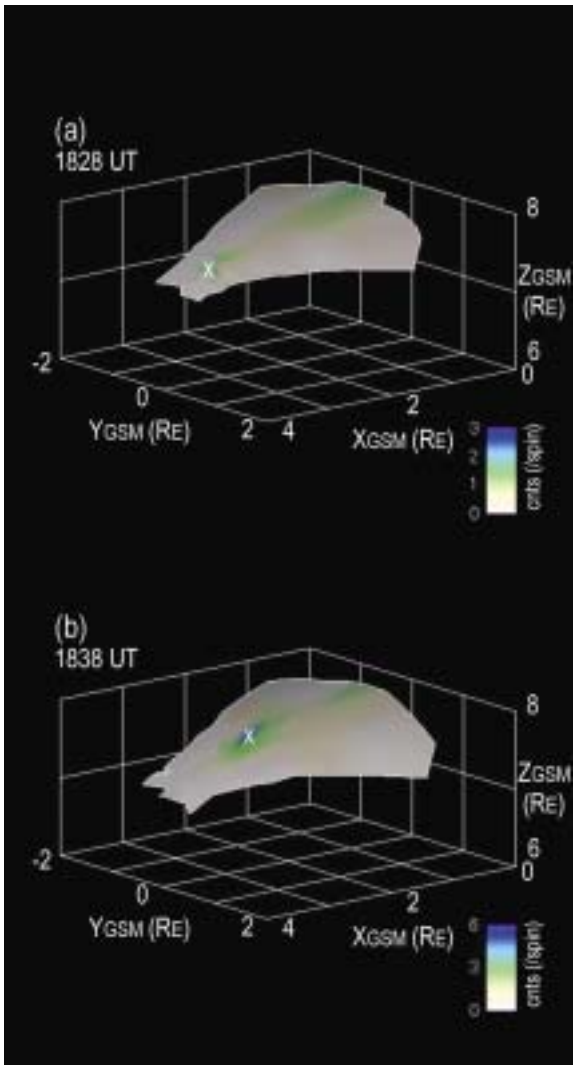
(a)
1828 UT
8
ZGSM
(RE)
6
0
-2
0
YGSM (RE)
2
4
2
XGSM (RE)
cnts (log10)
(b)
1838 UT
8
ZGSM
(RE)
6
0
-2
0
YGSM (RE)
2
4
2
XGSM (RE)
cnts (log10)

Figure 4.

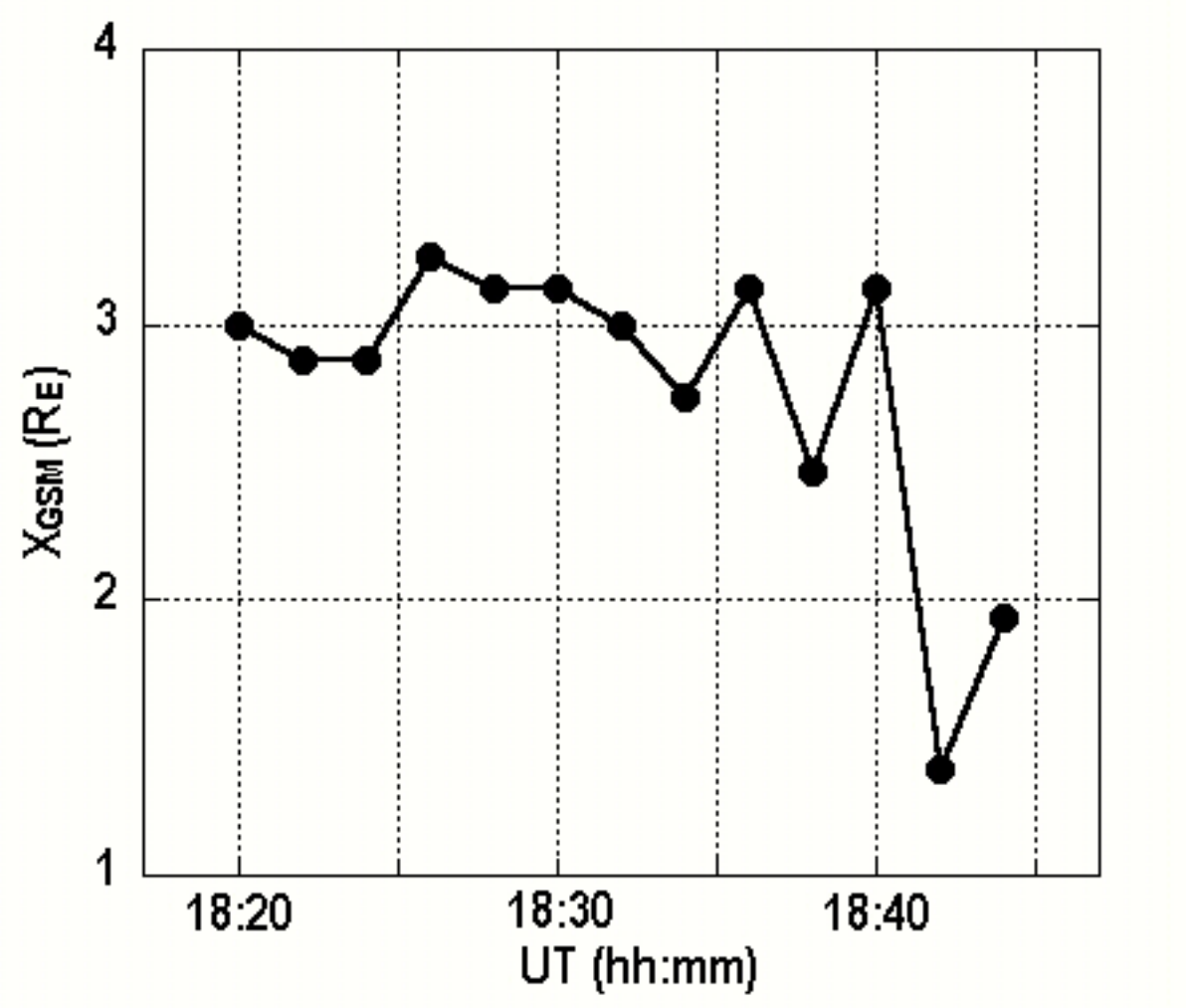

Figure 5.